ADVANCED QUANTUM TECHNOLOGIES
www.advquantumtech.com

Solid-State Qubit as an On-Chip Controller for Non-Classical Field States

*Roman V. Zakharov, Olga V. Tikhonova, Nikolay V. Klenov, Igor I. Soloviev, Vladimir N. Antonov, and Dmitry S. Yakovlev**

A basic element of a quantum network based on two single-mode waveguides is proposed with different frequencies connected by a solid-state qubit. Using a simple example of a possible superconducting implementation, the usefulness of the simplifications used in the general theoretical consideration has been justified. The non-classical field in a single-mode with a frequency of ω_1 is fed to the input of a qubit controller and transformed into a non-classical field in an output single-mode with a frequency of ω_2. The interface can establish a quantum connection between solid-state and photonic flying qubits with adjustable pulse shapes and carrier frequencies. This allows quantum information to be transferred to other superconducting or atomic-based quantum registers or chips. The peculiarities of the wave-qubit interactions are described, showing how they help to control the quantum state of the non-classical field. On this basis, the operating principles of solid-state and flying qubits for the future quantum information platforms are considered.

1. Introduction

Building a large-scale quantum computer is one of the most complex areas within quantum information technologies.[1–4] In modern quantum computing systems, information is typically encoded in the states of either solid-state qubits (artificial atoms) or photons (flying qubits). Each approach has its strengths and weaknesses. A "third way" of development is when relatively easily controlled solid-state qubits are responsible for information processing, and non-classical electromagnetic fields are responsible for information transfer across and between chips. But to bring such an approach to practice, we need to teach solid-state qubits to control non-classical electromagnetic fields.

Such an approach can be implemented on various technological platforms, including, for example, superconducting artificial atoms connected by high-quality resonators (cavities).[5–20] Our interest is invoked by the possibility of realizing a robust and targeted interaction[21–27] between a specific "atom" and a "field in a microcavity" ("SA+F" system). It is also possible to control (even directly during the interaction) the characteristics of the atom and the field. This control handle arises from the specifics of macroscopic interference in superconducting circuits with Josephson Junctions (JJ). JJs also give nonlinear scattering of microwave photons, similar to scattering processes in nonlinear optical media.[28,29] In both classical and quantum limits, superconducting atoms effectively interact with non-classical fields and can even generate them.[30–33]

The mentioned features of the "SA+F" systems were clearly manifested in a series of sophisticated experiments in the field of quantum optics, including the dynamical Lamb effect and the dynamical Casimir effect.[34–36] The progress in sources and detectors of non-classical microwave radiation can potentially lead to the creation of a "quantum radar"[37–39] and a "quantum internet"[40–44] with the transfer of information between quantum computing systems using quantum fields. In this work, we describe how to control the quantum states of the non-classical fields, transfer them from one mode to another, and manage them by wave-to-qubit interactions.

An important feature of the proposed systems is the high sensitivity of superconducting atoms to external electromagnetic fields. This feature causes problems in quantum computers.

R. V. Zakharov, O. V. Tikhonova, N. V. Klenov
Faculty of Physics
Lomonosov Moscow State University
Moscow 119991, Russia

R. V. Zakharov, O. V. Tikhonova
Kotel'nikov Institute of Radio Engineering and Electronics of RAS
Moscow 125009, Russia

O. V. Tikhonova, I. I. Soloviev
Moscow State University
Institute of Nuclear Physics
Leninskie gory, GSP-1, Moscow 119991, Russia

V. N. Antonov
Skolkovo Institute of Science and Technology
Bolshoy boul, 30, Moscow 121205, Russia

D. S. Yakovlev
Laboratoire de Physique et d'Etude des Matériaux, ESPCI-Paris
PSL Research University
Paris 75005, France
E-mail: dimitry.yakovlev@espci.fr

The ORCID identification number(s) for the author(s) of this article can be found under https://doi.org/10.1002/qute.202400141

DOI: 10.1002/qute.202400141

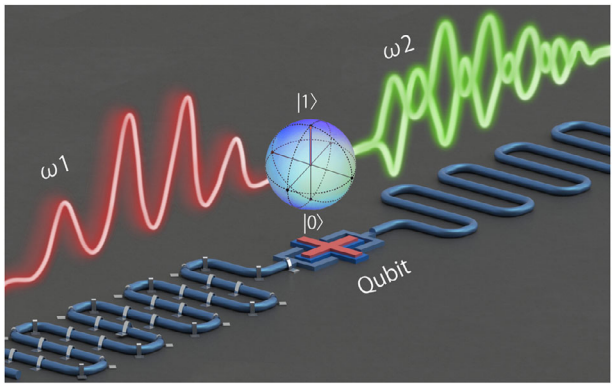

Figure 1. Principal scheme of the quantum controller: two waveguides for the input and output signals are connected to an artificial atom (qubit). The characteristic frequencies of the waveguides are slightly different from each other.

However, it can be used constructively in "quantum controllers" in distributed networks,[45] multi-chip systems,[46] and (more generally) physical systems that require encoding of higher dimensional quantum information.[47–58] We look at the abilities of the quantum controllers[59–61] and explore the analytical methods in this area.

2. Exemplification Example: Validating Theoretical Assumptions

We propose a general theoretical framework for a quantum controller of non-classical electromagnetic fields, which can potentially be applied to various practical realizations of such a system. In our analytical treatment, however, we have made several simplifying assumptions, the validity of which we demonstrate through a relatively simple example of the qubit controllers and waveguides for microwave photons.

To illustrate the experimental realization of the controller, we introduce a waveguide-qubit-waveguide system, as shown in **Figure 1**. The system consists of a superconducting X-mon qubit placed in a cavity and connected with two waveguides. The circuit design and microphotographs, specifically with the widely used "planar" X-mon qubit,[62] are shown in **Figure 2**b–e. The system seems to be quite similar to the one used in ref. [63], where two waveguides are connected to an artificial molecule composed of two interacting superconducting transmon qubits. In our case, we use high-quality single-mode waveguides, each supporting only one frequency mode. The experimentally measured frequency spectra of the two waveguides are shown in Figure 2f and can be seen to be very narrow, clearly demonstrating a single-mode regime. The cavity is tuned to support both frequency modes, allowing both fields to interact with the qubit simultaneously. For our purposes, the single mode of the transmission line waveguide can be approximated by an LC tank model, as shown in Figure 2a, using a lumped element approach.[64] To improve modeling accuracy, additional LC tank circuits can be considered for multiple modes in a more complex resonator.[65,66]

Note that in the implementation under consideration, the spectrum of the controller can be configured: The flux bias line facilitates the application of magnetic flux to the SQUID loop of the X-mon, thus changing its operating frequency. Two coplanar waveguide (CPW) transmission lines are capacitively coupled to the controller. Each is terminated at the resonator and ends with an open or short circuit to the ground.

While employing a CPW is straightforward in design and fabrication, it occupies a significant area. For instance, the CPW length is on the order of wavelength λ, corresponding to several millimeters for mode frequencies in the 6–8 GHz range (see Figure 2b,f, and **Table 1**). Future integration methods, such as flip-chip integration[67] or through-silicon vias,[68] are expected to be utilized in quantum networks.

We investigated the interconnected Xmon-based tunable element comprising two islands coupled via capacitance, depicted in Figure 2b. The system configuration, illustrated in Figure 2c,d, consists of a Josephson SQUID junction (see Figure 2d), linked by a capacitance in the form of two thin-film pads on opposite sides of the junction. Our investigations involved measurements employing a cavity microwave resonator containing an X-mon. The critical components of this superconducting element are submicron-scale Josephson superconductor-insulator-superconductor (SIS) tunnel junctions, as demonstrated in Figure 2e. These junctions are manufactured using shadow deposition[69,70] through two-layer electron-resist masks generated by electron lithography. The tunnel barrier is formed by the controlled oxidation of the lower aluminum S-layer inside the high-vacuum system's chamber. Tunnel SIS junctions with lateral dimensions ranging from 50 to 1000 nm, critical currents I_c between 5 nA to 10 μA (the critical current densities ranging from 0.05 to 4 kA cm^{-2}) were fabricated. Nota bene: the dimensions of such a structure are minor compared to the wavelength of the waveguides used.

One- and two-tone spectroscopy is used to determine the qubit frequency (ω); during this step, one also gets accurate estimates of the CPW frequencies (ω_1, ω_2) and the resonator-qubit coupling strengths $\Gamma_1 = \Gamma_2 = \Gamma$. To get complete insights into the system's functionality, measuring the qubit's coherence times concerning its magnetic field shift is crucial.Stability of system characteristics versus detuning from the sweet spot is important. Critical parameters such as energy relaxation times T_1, phase relaxation times $T_2{}^*$, and echo coherence time T_{2E} were assessed from both sides of the qubit (see Table 1). The results in Figure 2g show the coherence times measured versus the distance from the sweet spot (SWS). Using a magnetic field loop directly linked to the element provides detuning. The measured average coherence times ranged between 5 and 25 μs. In our tunable Xmon-based setup, the T_1, $T_2{}^*$, and T_{2E} times remain constant throughout the measured half-flux-quantum range (see Figure 2g and Table 1). When two waveguides with different frequencies are connected to a single qubit, their quality factors remain at the 5×10^5 level (Table 1). Moreover, the coherence times remain constant instances, regardless of swapping the drive and readout CPW. We conclude that the waveguides do not interfere with each other and that no uncontrolled energy dissipation is observed in our system. This preliminary characterization of the waveguide-qubit-waveguide system provides a solid basis for the theoretical description of the on-chip quantum controller for non-classical field states presented in the following sections.

The potential experiment should include a superconducting qubit for generating non-classical electromagnetic fields, a qubit

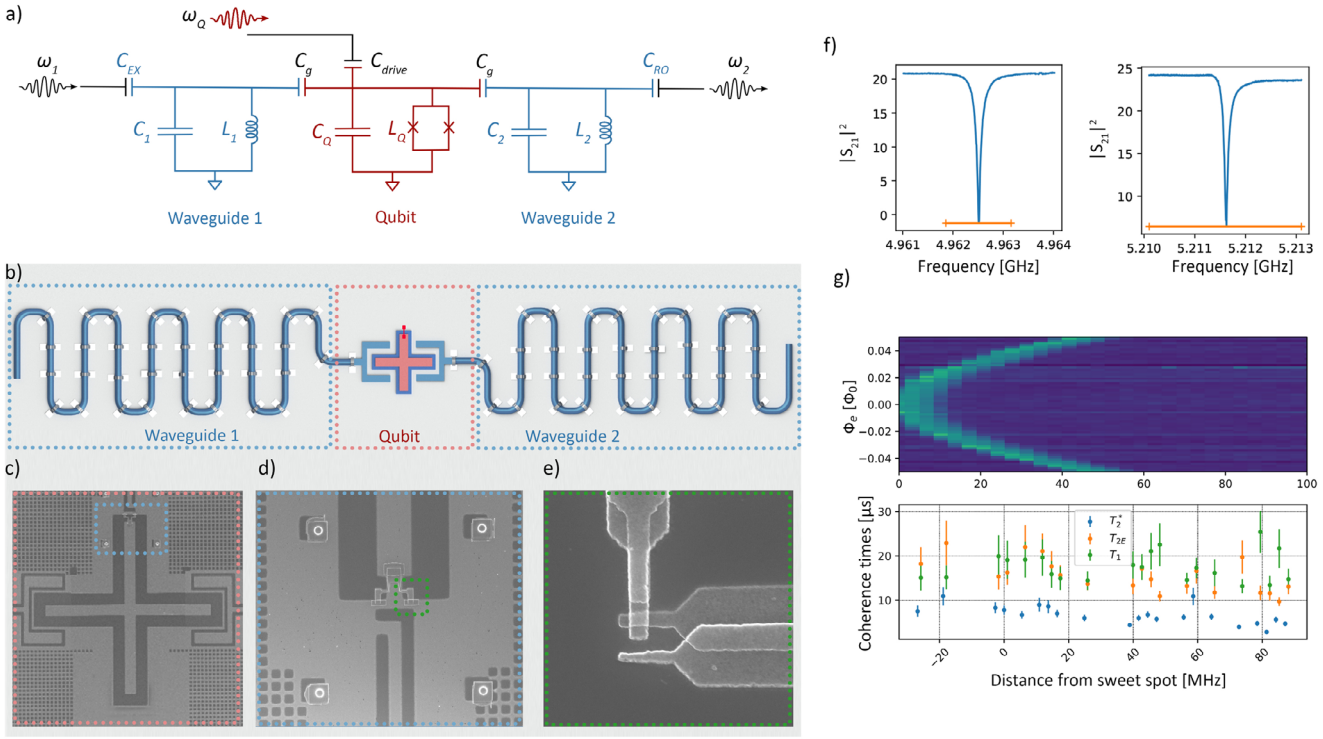

Figure 2. a) Equivalent lumped element circuit model of the device; b) Schematic view of a planar superconducting waveguide-qubit-waveguide system. The device consists of an X-mon qubit (highlighted in red) with two Josephson junctions and a large capacitive shunt coupled to two CPWs (highlighted in blue); c) shunting capacitor for Xmon-based element with capacitance C_{sh}; and d) microwave line for controlling the qubit frequency and X-mon SQUID; e) One of two Josephson junctions of SQUID; f) Spectroscopic test results for the waveguides; g) Quantum controller stability test results: qubit decoherence time versus magnetic flux tuning.

controller for precise state manipulation, and a detector for field measurement.

3. Method of Analytical Description of State Dynamics in Basic Element

Summarizing the results of preliminary experiments, we describe the basic element of an "all-quantum" computing system as follows: a non-classical field in a single-mode waveguide with a frequency of ω_1 is fed to the input of a qubit-controller and turns into a non-classical field in an output single-mode CPW with a frequency of ω_2. At the first stage of theoretical consideration, we will consider the controller as a two-stage system with a frequency of ω. The system Hamiltonian is a sum of free Hamiltonians for fields, qubit, and the interaction terms:

$$H = \hbar\omega_1 a_1^\dagger a_1 + \hbar\omega_2 a_2^\dagger a_2 + \frac{1}{2}\hbar\omega\sigma_z + \\ + \hbar\Gamma_1(\sigma^+ a_1 + \sigma^- a_1^\dagger) + \hbar\Gamma_2(\sigma^+ a_2 + \sigma^- a_2^\dagger) \quad (1)$$

As we move toward the practical implementation of quantum networks, it will be imperative to account for the real dispersion in waveguides[71,72] by including terms in the overall Hamiltonian that correspond to different modes with their respective frequencies.

The state of our simplified system can be expanded over eigenfunctions of the non-interacting qubit and field subsystems as follows:

$$\psi = \sum C^g_{n_1 n_2}(t)\,|g\,n_1\,n_2\rangle + \sum C^e_{n_1 n_2}(t)\,|e\,n_1\,n_2\rangle \quad (2)$$

where the symbols g, e refer to the ground and excited states of the qubit; n_1, n_2 are the photon numbers in each field mode.

The time-dependent differential equations for the probability amplitudes of the interaction-free states contributing to the total solution are given by:

$$\frac{dC^g_{n_1 n_2}}{dt} = -i\Gamma_1\sqrt{n_1}e^{i(\omega_1-\omega)t}C^e_{n_1-1\,n_2} - \\ -i\Gamma_2\sqrt{n_2}e^{i(\omega_2-\omega)t}C^e_{n_1\,n_2-1}$$

Table 1. Overview of the system parameters.

ω_W, GHz	$Q_i \times 10e^5$	ω_Q, GHz	Γ, MHz	T_1, μs	T^*_2, μs	T_{2E}, μs
$\omega_1 = 4.96$	4.84	$\omega = 4.64$	35 ± 2	19.99	8.91	15.22
$\omega_2 = 5.21$	4.91		34 ± 2	19.74	8.83	14.98

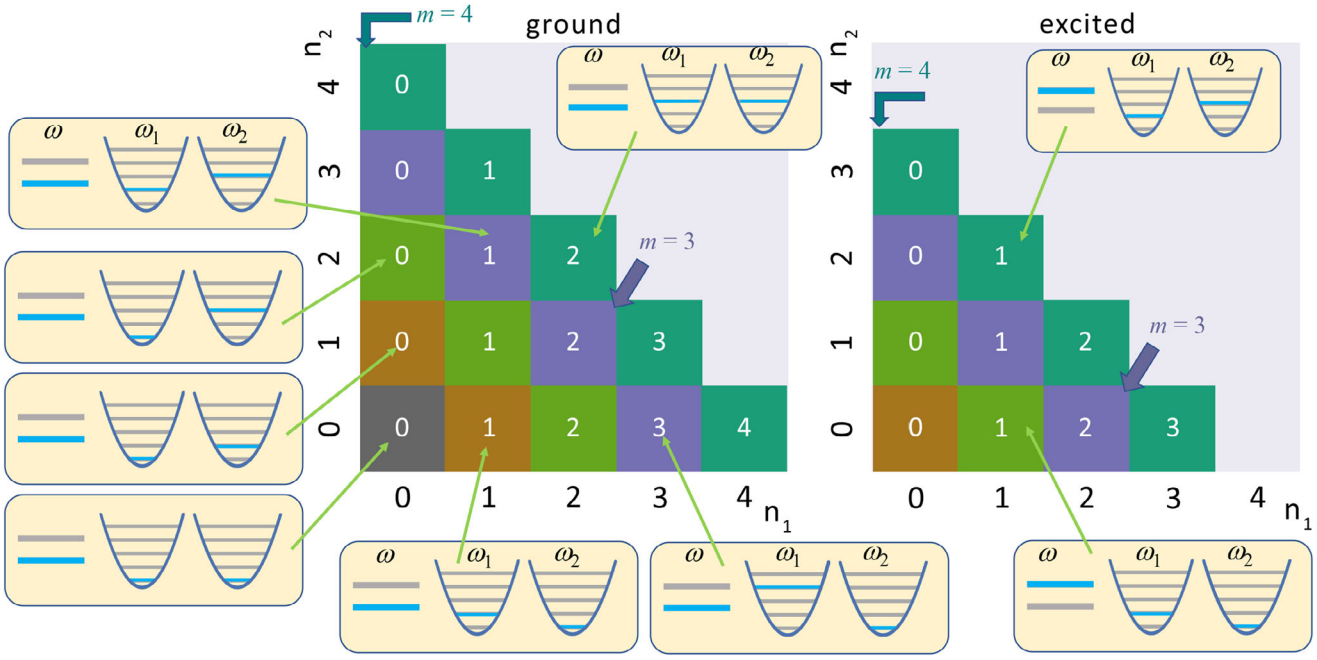

Figure 3. The structure of states of the system consisting of two fields (n_1 and n_2 are the numbers of photons in these fields) and qubit (ground or excited). According to the system (4), all states are indexed with the total number of excitation in a given energy channel m and the number of photons in the first field mode. The states referred to the same energy channel are arranged in a diagonal and are indicated by the same color. The states marked by different colors are uncoupled during the time evolution described by the system (4).

$$\frac{C^e_{n_1 n_2}}{dt} = -i\Gamma_1\sqrt{n_1+1}\,e^{i(\omega-\omega_1)t}C^g_{n_1+1\,n_2} - \\ -i\Gamma_2\sqrt{n_2+1}\,e^{i(\omega-\omega_2)t}C^g_{n_1\,n_2+1} \tag{3}$$

If $\omega = \omega_1 = \omega_2$ the solution can be found analytically. In general case we have solved them numerically.

The solution of the system can be simplified by taking into account the found integral of motion $I_1 = a_1^\dagger a_1 + a_2^\dagger a_2 + \sigma^+\sigma^-$ which represents the total energy in the system. Since the total energy is conserved the interconnected Equations (3) appears to be a set of independent groups of equations specifically for each initial number of excitations m in the system which can be defined as follows: $m = n_q + n_1 + n_2$. Here, n_1 and n_2 stand for the photon numbers in two field modes, while n_q equals 1 or 0 for the excited or ground qubit state, respectively.

For any given value of the parameter m, the corresponding set of equations can be solved separately, even if the initial field state is chosen as a broad superposition of different photon number states. For this reason, it is more convenient to renumber the tripartite basis states and to characterize them additionally to the qubit indices "g" and "e" by the total number of excitations m and the number of photons in the first mode n_1. The corresponding number of photons in the second field mode can be found automatically as $n_2 = m - n_1 - n_q$. Such a procedure is very useful for parallel calculations and leads to the following set of $(2m+1)$ equations obtained for each "energy channel" with a given value of the parameter m:

$$\frac{dC^g_{mj}}{dt} = -i\Gamma_1\sqrt{j}\,e^{i(\omega_1-\omega)t}C^e_{mj-1} - i\Gamma_2\sqrt{m-j}\,e^{i(\omega_2-\omega)t}C^e_{mj} \\ j = 0, 1, \ldots, m$$

$$\frac{dC^e_{mj}}{dt} = -i\Gamma_1\sqrt{j+1}\,e^{i(\omega-\omega_1)t}C^g_{mj+1} - i\Gamma_2\sqrt{m-j}\,e^{i(\omega-\omega_2)t}C^g_{mj} \\ j = 0, 1, \ldots, m-1 \tag{4}$$

Figure 3 shows the classification of states taking into account the channels of their possible formation. Later, when analyzing the results, we will normalize the time by the inverse coupling constant between the qubit and the resonator, Γ^{-1}.

It should be emphasized that the contribution of a given energy channel with fixed m is determined by the weight of this channel in the initial state of the system and does not change during the interaction. Thus, it is possible to neglect some energy channels without affecting others. For these reasons, the developed theoretical approach seems very promising and gives many advantages due to the possibility of analyzing the physical processes in different energy channels independently.

4. Results and Discussion

4.1. Quantum Field State Generation and Transfer

Here, we present a systematic review of the results for the "SA+F" system used as a generator of a quantum state in an

output field mode depending on the input. The simplest example is state transfer, where the given state is initially in mode ω_1, and we want to transfer it to mode ω_2.

Note that this is a difficult task. Usually, not only the state but even the photon statistics of the field can hardly be transferred from mode to mode. We will now demonstrate a method to circumvent this issue.

We will consider low photon number states, which are truly non-classical with quantum uncertainties playing an important role. A simple example is the fixed photon number (Fock) state of the field or the low photon number coherent state. The coherent field state can be generated with multiple qubits connected to a resonator if they are coherently excited.

The regime of high-quality transfer from one field mode to another can be achieved only if the difference between the frequencies $\delta = |\omega_1 - \omega_2|$ is much less than the interaction strength $\delta \ll \Gamma_i$ since the number of excitations is invariant and the energy conservation constraint exists.

Two different regimes of field-qubit interaction are found, determined by the ratio between the field-qubit interaction strength and the detuning of the mean-field frequency from the qubit resonance transition:

$$\Delta = \omega - \frac{\omega_1 + \omega_2}{2} \tag{5}$$

For efficient field state transfer, the interaction strengths Γ_1 and Γ_2 should be rather close to each other, such that $\Gamma_1 \approx \Gamma_2 = \Gamma$. In the regime of weak field-qubit interaction (see **Figure** 4a), the qubit frequency is far from the field frequencies, so Δ is much larger than the effective interaction $\Gamma\sqrt{\langle n\rangle + 1}$, where $\langle n\rangle$ is the average photon number in the field. In this case, there is almost no excitation of the qubit, and its upper level is mostly empty all the time (see Figure 4b). Thus, all the energy in the system is exchanged between the field modes, but it's important to note that this exchange is only possible due to the interaction with the qubit. In this regime, the qubit acts as a good transmitter between the two field modes.

In the opposite regime, $\Delta \leq \Gamma\sqrt{\langle n\rangle + 1}$, the energy exchange between the field modes also takes place, but their mean photon numbers oscillate rather fast with a relatively large amplitude (see Figure 4c) due to high qubit excitation. In this case, one has to stop the interaction at the right moment to get the desired field state in the second mode (but this can be quite a challenge).

In this paper we will also consider only the first regime of non-resonant weak field-qubit interaction, since it is more suitable for high-quality transfer and generation of the non-classical field states.

To analyze the obtained results, it is important to work out the criteria that show that the state transfer procedure is good enough. First, we need quantitative metrics to analyze the quality of the generated state in the output mode. Let us suppose that initially, we have an input state in the first field mode, which is a superposition of different Fock states, and there are no excitations in the second mode and in the qubit:

$$|\psi(t=0)\rangle = \sum_{n_1} C_{g,n_1,0}(t=0)\,|gn_1 0\rangle \tag{6}$$

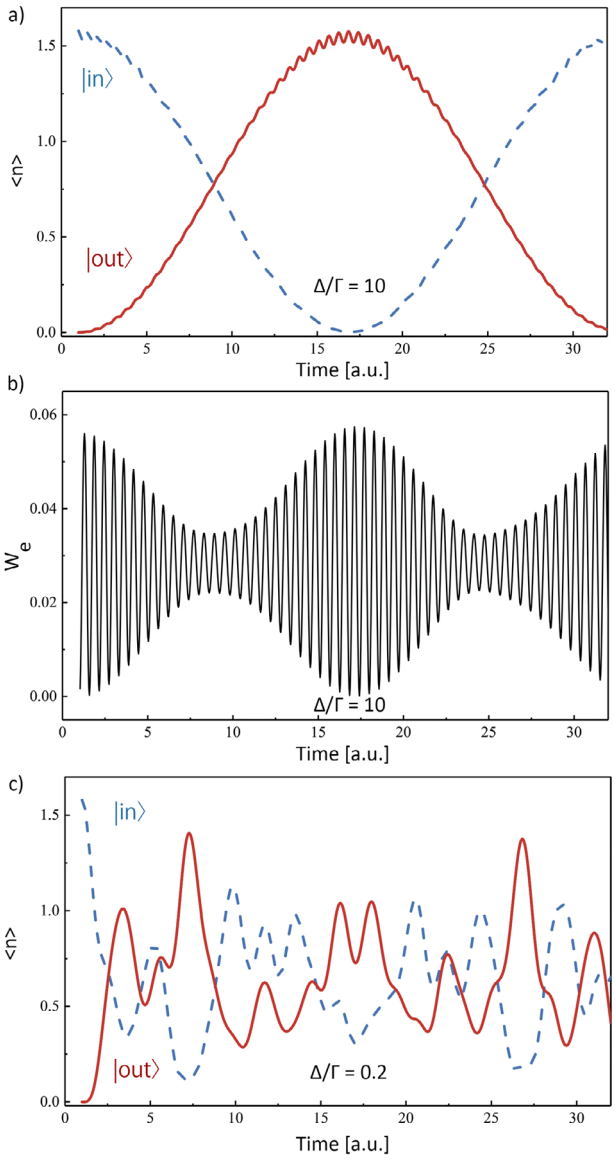

Figure 4. Evolution of average photon number of two field modes, blue dashed for the input field with ω_1, red solid for output field with ω_2, obtained for the initially coherent state of the first field mode with mean photon number 1.6 and ground state of the qubit at $(\omega_2 - \omega_1)/\Gamma = 0.005$ in the regime of weak (strongly non-resonant) field-qubit interaction, $\Delta/\Gamma = 10$ (a) and strong field-qubit interaction, $\Delta/\Gamma = 0.2$ (c). Figure (b) shows a very small qubit excitation in the weak interaction regime. The time is given in units of $\frac{1}{\Gamma}$; 1 a.u. $\approx$ 28.57 ns in our system.

In the most general case, the evolution of this state overtime during the interaction can be represented as follows:

$$|\psi(t)\rangle = \sum_{a,n_1,n_2} C_{a,n_1,n_2}(t)\,|an_1 n_2\rangle \tag{7}$$

where the indices $a = g, e$ characterize the qubit state.

Let's assume that we want to transfer the photon number statistics from the input state to the second field mode. The

probability of finding k photons in the output mode at a given time is given by:

$$|C_k^{red}(t)|^2 = \sum_{a,n_1} |C_{a,n_1,k}(t)|^2 \tag{8}$$

If we don't stop the interaction at the right moment, some energy will remain in the first (input) field mode and the state transfer will not be perfect. Therefore, we can define the transfer error metrics as the difference between the probabilities of finding k photons in the second field mode at certain time t and in the first mode at the initial moment, and further sum over all photon numbers:

$$\sum_k Error_k(t) = \sum_k \left| |C_k^{red}(t)|^2 - |C_{g,k,0}(0)|^2 \right| \tag{9}$$

It is easy to show that $\sum Error_k \leq 2$. So we can define the transmission quality as

$$quality(t) = 1 - \frac{\sum Error_k(t)}{2} \tag{10}$$

where 1 corresponds to the ideal metrics transfer, and 0 means that the field statistics in the modes have nothing in common.

Another important metrics is the purity of the second field state:

$$purity(t) = Tr(\rho_{red}^2(t)) \tag{11}$$

where $\rho_{red}^{i,j} = \sum_{a,n_1} C_{a,n_1,i} C_{a,n_1,j}^*$

When the purity is close to unity, the field in the second mode is characterized by a certain wave function, which seems to be a necessary condition for high-quality state transfer. In the following, we will focus on the possibility of transferring typical nonclassical field states.

4.2. Transfer of Fock States and Generation of NOON States

Let us first discuss the transfer of the Fock state (the state with a certain number of photons) from one field mode to another. In the case of the one-photon state, the situation is quite simple. At any point in time, the two-mode field can be in the state $|10\rangle$ or $|01\rangle$, or in a superposition of both. The time-dependent populations of these two states are depicted in **Figure 5a**; these curves show an almost complete transfer of a photon from one field mode to the other, achieved by the time $t = 16.5$ a.u. (the time is given in units of $\frac{1}{\Gamma}$; 1 a.u. $\approx$ 28.57 ns in our system). Indeed, the corresponding time-dependent purity and quality are found to approach unity at this time (see Figure 5b). It is found that the observed one-photon transfer repeats periodically in time.

For the two-photon initial state, the transfer procedure can also be performed with high quality. In this case, however, more different bipartite field states can be populated during the interaction. Their populations as a function of time are shown in Figure 5c. It should be emphasized that the purity of the state in the second mode changes strongly during the interaction, approaching its minimum value of 0.5 twice per period of quality oscillations.

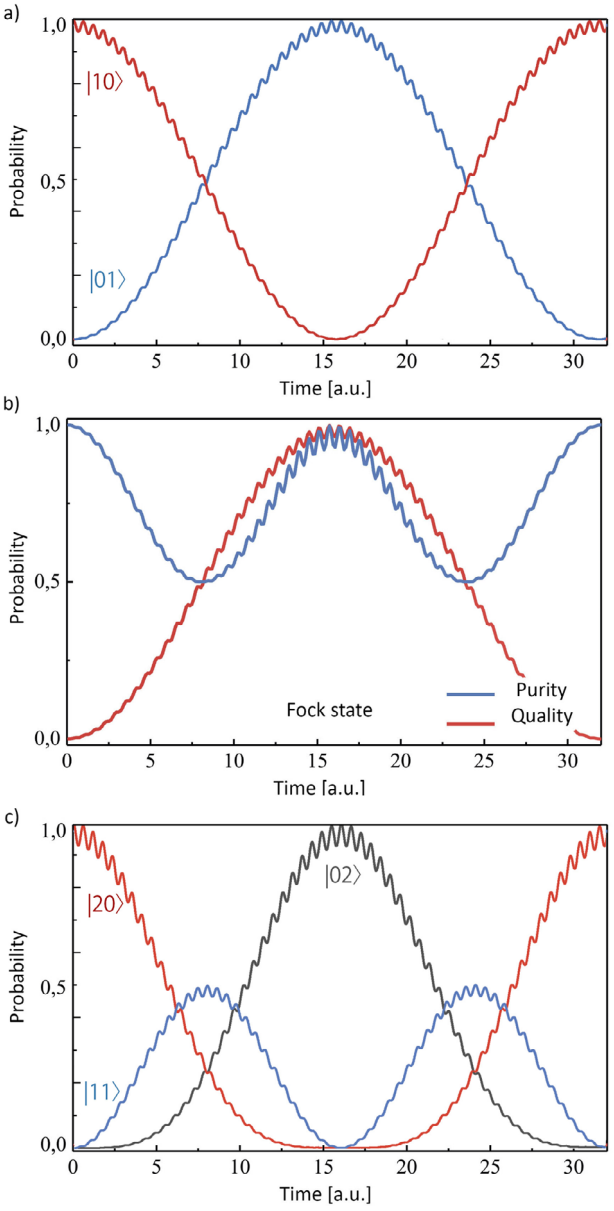

Figure 5. Fock state transfer from one field mode to another. The time-dependent populations of different bipartite field states formed during the interaction with the qubit in the case of one-photon transfer (a) and two-photon state transfer (c); the quality and purity metrics of the one-photon transfer procedure as a function of time (b).

This is a clear indication of the formation of strongly entangled two-mode field states.

We have found that the so-called N00N-states can be generated during the field-qubit interaction. Such states are highly entangled and describe the case when there are N photons in one field and a vacuum in the second one or vice versa: $|N00N\rangle = (|N0\rangle + |0N\rangle)/\sqrt{2}$ with different possible relative phases in such superposition. N00N-states are desired because they hold great promise for important practical applications in quantum information technology. **Figure 6** illustrates the types of different NOON states formed during the Fock state transfer by the time

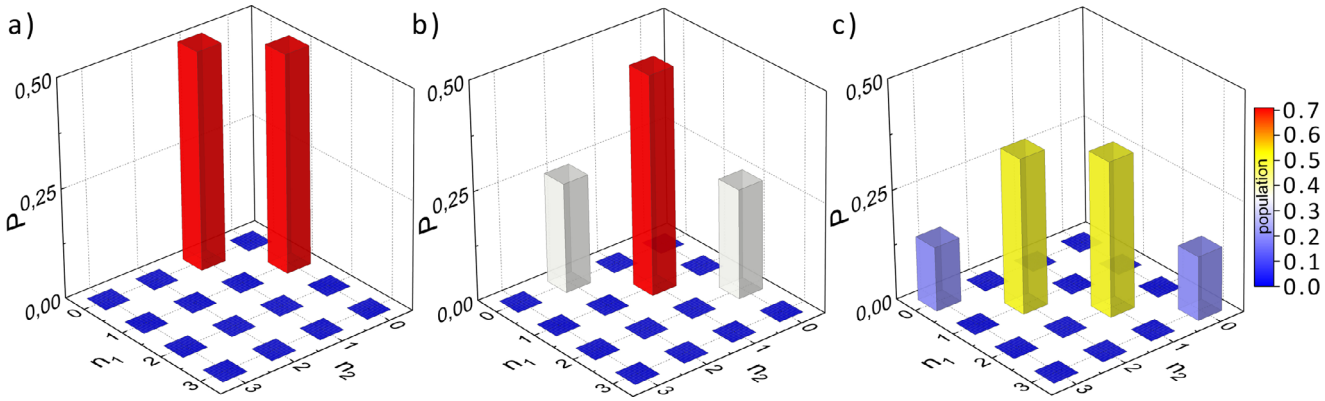

Figure 6. The NOON states generated during the transfer of different Fock states at the time corresponding to the minimum purity in Figure 5 for different initial conditions: $n_1 = 1$ (a), $n_1 = 2$ (b), and $n_1 = 3$ (c).

corresponding to the minimum of purity. In the case of single-photon transfer, only the superposition of $(|10\rangle + i\,|01\rangle)/\sqrt{2}$ with relative phase equal to $\pi/2$ can be obtained.

For two-photon initial state the $(|2\rangle\,|0\rangle + |0\rangle\,|2\rangle)/\sqrt{2}$ state can be found. For initial Fock states with higher numbers the set of possible entangled states is richer. Specifically, during the transfer of the 3-d Fock state the superposition $\gamma\,(|3\rangle\,|0\rangle + |0\rangle\,|3\rangle) + i\beta\,(|2\rangle\,|1\rangle + |1\rangle\,|2\rangle)$ can be generated (Figure 6c). It should be noted that the generation of entangled Bell states, which can also be called NOON states with $N = 1$, has been achieved in a rather similar setup using two superconducting transmons.[63]

Thus, the high-quality transfer of different Fock states from one field mode to another is demonstrated. The transfer is accompanied by the formation of the N00N states, which are mostly pronounced at the minimum of purity.

4.3. Transfer of Coherent Field State

In this subsection, we focus on the transfer of the coherent state with a small average number of photons from one field mode to another. The coherent state is known to be the following superposition of many Fock states:

$$|\psi_c\rangle = e^{-|\alpha|^2/2} \sum_n \frac{\alpha^n}{\sqrt{n!}} |n\rangle \tag{12}$$

This state is characterized by the Poisson distribution over photon numbers with a mean value equal to $|\alpha|^2$. An example of the statistics transfer from mode to mode due to field-qubit interaction is shown in **Figure 7** for the initial coherent state with $\alpha = 1.5$. At the beginning ($t = 0$) photons are present only in the first field mode and the Poisson photon distribution is well seen in Figure 7a, at the intermediate stage ($t = 8\,a.u.$) we get photons in both modes (Figure 7b).

At the final moment ($t = 16.5\,a.u.$), all the energy appears in the second field mode, with the photon number distribution found to coincide almost perfectly with the initial Poisson distribution of photons of the input state (compare Figure 7a,c). Thus, the photon statistics are fully transmitted to the second mode (Figure 7c). However, the relative phases between different Fock states are found to be changed: initially, they were chosen equal to zero(since α is real) while at $t = 16.5\,a.u.$ the phase difference of π between adjacent photon number states appears (see Figure 7d). So, the final state isn't a full copy of the initial state in the input mode. Usually, the relative phases of states in a superposition are very important due to their dramatic influence on the shape of the probability density distribution of the coordinate or momentum quadrature. However, such a problem does not arise in our case. The acquired relative phase shift between Fock states indicates only that the coherent state with parameter $(-\alpha)$ instead of α is generated in the second field mode. In coordinate representation such wave-packet corresponds to the field state prepared initially in the first mode but with opposite coordinate field quadrature: $\psi_{out}(x) = \psi_{in}(-x)$. Thus, the coherent state is shown to be successfully transferred without distortion.

The quality of the transmission procedure and the purity of the state in the second field mode are shown in **Figure 8a**. The quality parameter is found to reach almost unity at $t_{tr} \approx 16.5\,a.u.$ and remains above 0.9 within the time interval of $\delta t \approx \pm 2\,a.u.$ around this point.

It can be seen that the maximal quality of the transfer is achieved at approximately the same time point as it is obtained in the case of the initial Fock state. In addition, for integer ratio Δ/Γ, the dynamics of the system are characterized by periodic oscillations of energy and states between two field modes. The period of such oscillations (or the revival time) can be estimated analytically in the limit of degenerate field frequencies. Under such approximation it is more convenient to describe the interaction in terms of the sum and difference field modes characterized by the following photon operators:

$$b_1 = \frac{\Gamma_1 a_1 + \Gamma_2 a_2}{\Gamma_{eff}},\ b_2 = \frac{\Gamma_2 a_1 - \Gamma_1 a_2}{\Gamma_{eff}},\ \Gamma_{eff} = \sqrt{\Gamma_1^2 + \Gamma_2^2} \tag{13}$$

It can be seen from the Hamiltonian (1) that only the sum mode interacts with the qubit with efficiency Γ_{eff}, while the difference mode is not coupled with qubit at all. For this reason actually the non-resonant quantum Rabi oscillations take place with the Rabi frequency $\Omega_n = \sqrt{\Gamma_{eff}^2 n + \frac{\Delta^2}{4}}$ for each initial Fock state. The total revival of the whole field state in the first field mode is found

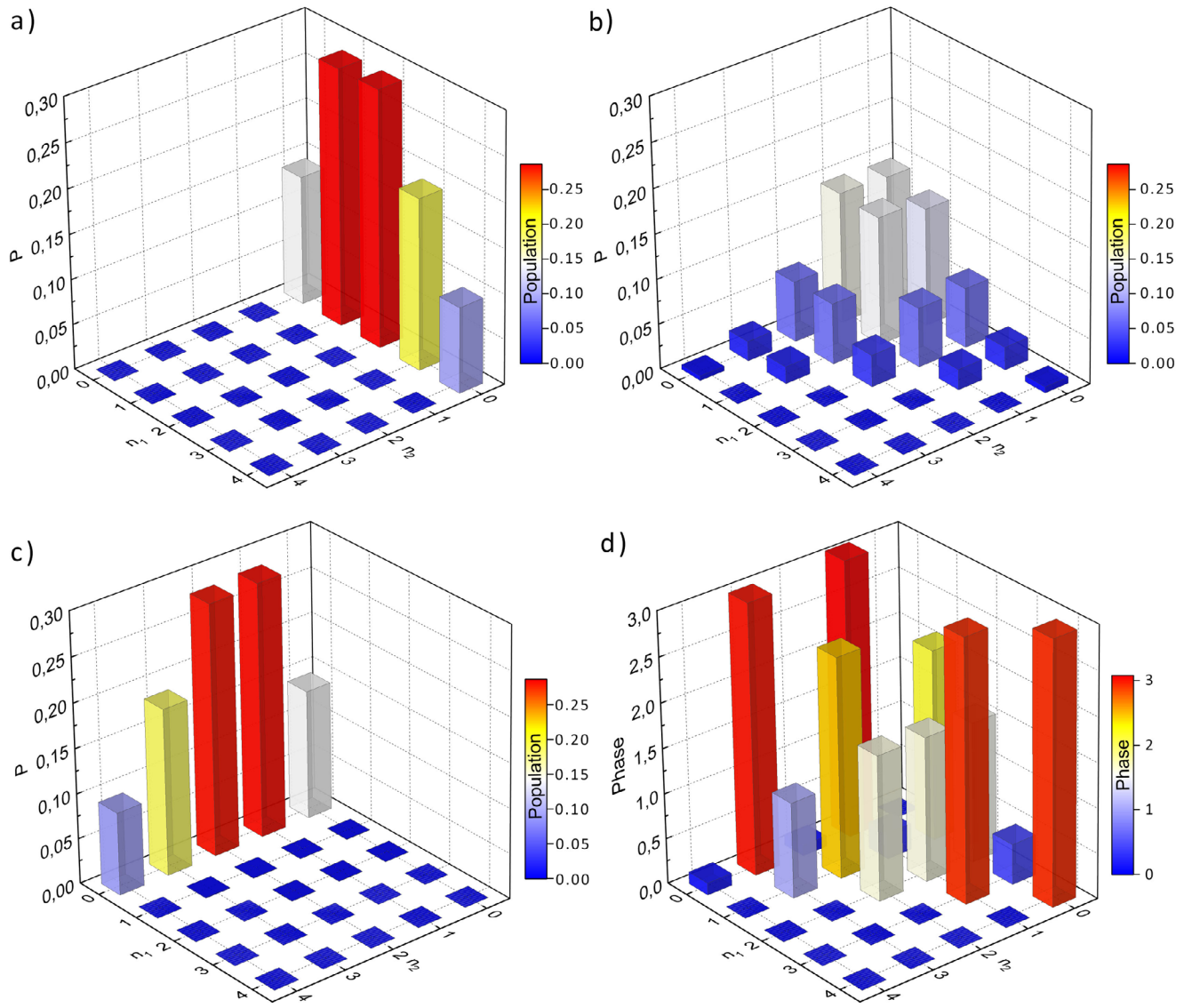

Figure 7. The evolution of the photon number distribution in two field modes obtained at different times during the transfer of the coherent state with $\alpha = 1.5$ is shown at the beginning (at $t = 0$) (a), in the middle (b) and at the end (c) of the transfer procedure. The phases reached by each Fock state at the end of the transfer are shown in figure (d). The parameters used are $(\omega_2 - \omega_1)/\Gamma = 0.005$, $\Delta/\Gamma = 10$.

to occur if only the amplitudes and phases of all Fock states will return to their initial values, specifically at time T_{rev} obeying the condition $(\Omega_n - \Omega_{n-1})T_{rev} = 2\pi$. In the considered non-resonant case the Rabi frequency weakly depends on the Fock number n leading to the simplest estimation (in the first order on the ratio $\frac{\Gamma}{\Delta}$) of the revival time as $T_{rev} \sim \pi\frac{\Delta}{\Gamma^2} = 10\pi\ a.u.$ (in units of $\frac{1}{\Gamma}$). It is evidently seen from Figures 4, 5, and 8 that the time of the best state transfer to the second field mode t_{tr} appears to be equal to one half of the revival period and then can be estimated as $t_{tr} \sim \pi\frac{\Delta}{2\Gamma^2} = 5\pi\ a.u.$ This value appears to be in good agreement with our obtained results.

By taking into account the second-order corrections to the estimation of t_{tr} we get a small increase of this value due to dependence on the mean number of photons $\langle n\rangle$ in the field: $t_{tr} \approx \pi\frac{\Delta}{2\Gamma^2}\left(1 + 4\langle n\rangle\frac{\Gamma^2}{\Delta^2}\right) \approx 16.5\ a.u.$ The found value perfectly coincides with the time of the best transfer demonstrated on Figure 4, 5, and 8. Thus, it is possible either to predict the time of the high-quality state transfer or to perform managing of this time by changing the frequency detuning and the strength of coupling with qubit.

4.4. Qubit as a Beam Splitter

Let us analyze the purity of the coherent state that is transferred to the second field mode. The results are presented in Figure 8 and evidently demonstrate that purity is close to unity during all the time of the interaction. This fact means that the fields in both modes are almost not entangled at any instant of time and can be characterized by pure states each with its own wave function. These pure states are found to be the coherent states

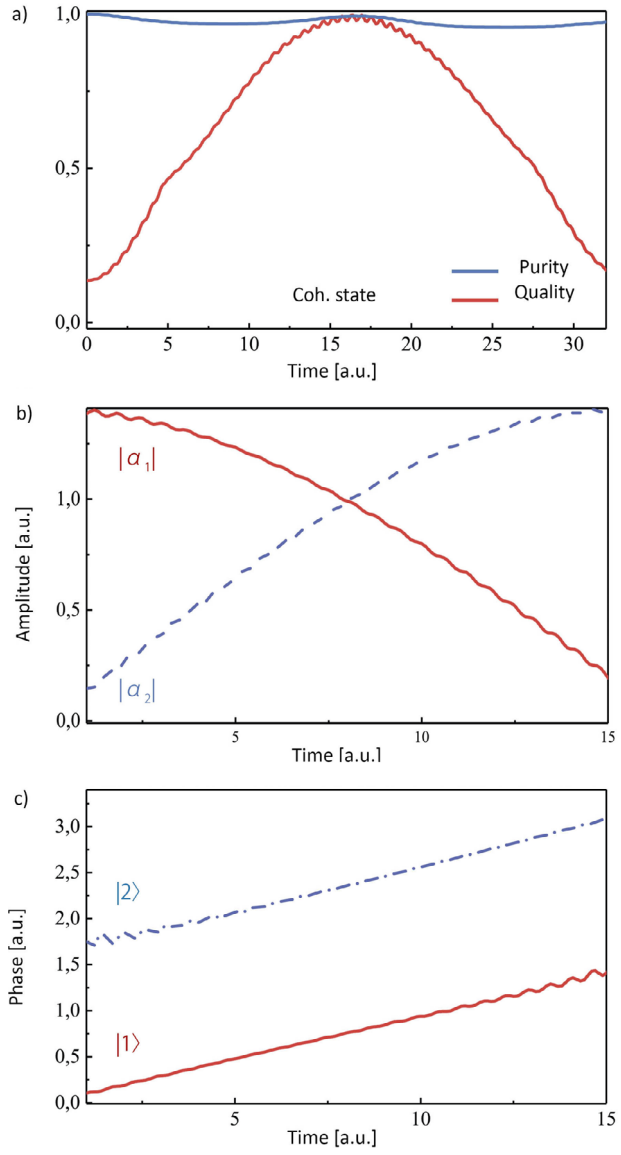

Figure 8. The quality of the transmission procedure. a) The purity of the state in the second field mode obtained during the transfer of the initial coherent state in the first field mode with $\alpha = 1.5$ for $\Delta/\Gamma = 10$. b,c) The time-dependent absolute values and phases of parameters α_1 and α_2 characterizing the coherent states of quantum fields in two modes during the off-resonant interaction with qubit.

characterized by parameters α_1 and α_2, which change over time. The time-dependent absolute values and phases of parameters α_1 and α_2 characterizing the coherent states of quantum fields in two modes, in this case, are presented in Figure 8b,c.

During the interaction with a qubit, the energy moves from one field mode to another, such as the mean number of photons decreasing in the first field mode and increasing in the second one. At the same time, each field always remains in a pure coherent state. As a result, starting from the initial coherent state in the first field mode, we obtain the generation of two new coherent states with fewer photon numbers changing with time. It should be emphasized that the observed energy exchange between quantum field modes is possible due to the interaction with the qubit only. Thus, in the considered regime the qubit acts like a beam splitter of microwave signals with transmission and reflection probabilities depending on time. Therefore, it is possible to vary the beam splitter balance by choosing the time point during the evolution.

It is interesting that though the phases of the obtained coherent states are also changing in time (see Figure 8c), the relative phase shift between the states remains constant and is found to be equal to $\pi/2$. For example, the bi-partite state obtained at half of the transmission time can be presented as follows:

$$|\psi_{mid}\rangle \approx \left|\frac{\alpha}{\sqrt{2}}\, e^{i\pi/4}\right\rangle_1 \times \left|\frac{\alpha}{\sqrt{2}}\, e^{i3\pi/4}\right\rangle_2 \tag{14}$$

Since the whole state appears to be a direct product of the individual states of each field, it is possible to manipulate or perform measurements independently in one or another field mode. Thus, due to interaction with the qubit, it is possible to generate different coherent states with required characteristics in two field modes. The strongly off-resonant character of the interaction leads to negligibly small excitation of the qubit and provides the regime when the qubit works as a transmitter of energy between field modes.

4.5. Measuring Field Phases

Note that the considered state generator of a non-classical electromagnetic field on a chip can be used for fine measurements.

Let's assume that we want to retrieve the relative phase ϕ of the initial input state of the field in the first mode with ω_1 by coupling it with qubit:

$$|\psi\rangle = \left(|\gamma||1\rangle + |\beta|e^{i\phi}|2\rangle\right)|0\rangle\left(\frac{|g\rangle + |e\rangle}{\sqrt{2}}\right) \tag{15}$$

Of course, we can do this without the help of the second field, which measures only an average signal (average number of photons) in the first field. However, it turns out that this value oscillates significantly with time due to the interaction with the qubit. Therefore, signals corresponding to different phases are close to each other and can hardly be distinguished. The error in the measurements can lead to completely wrong results. An example of such time-dependent signals is shown in **Figure 9a**.

In the presence of the second field mode, the situation becomes different. Both field modes interact with qubit simultaneously. At a certain instant of time, when the efficiencies of their interaction with qubits become close to each other, the total signal measured simultaneously in both field modes reveals the suppression of oscillations in time. In this regime, the signals obtained for different phases are found to be well-separated and can be distinguished (see Figure 9). In our case, the proper time interval is found between 7 and 9 a.u. when similar energies characterize both field modes. When there are more photons in the input field, the stable part in the curves shown in Figure 9 is much more pronounced, existing for longer time intervals, and the phase recovery becomes more reliable.

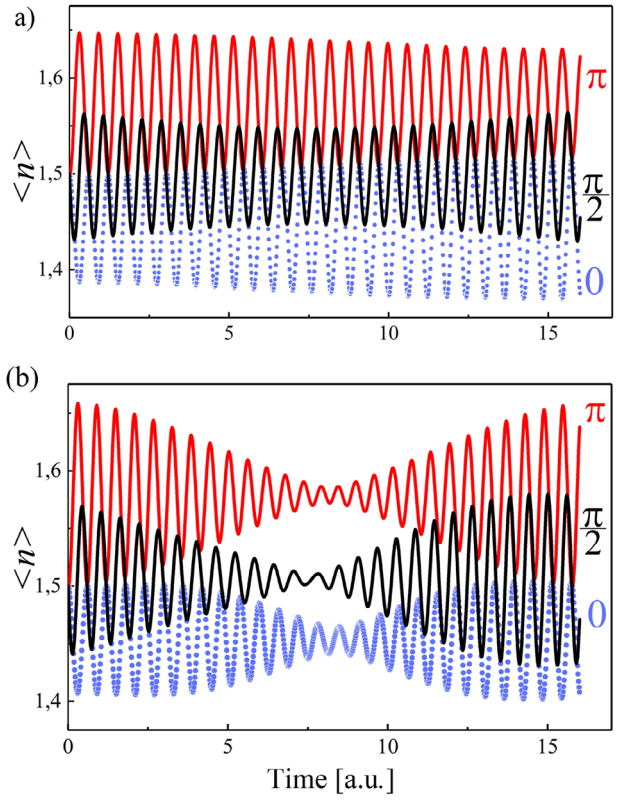

Figure 9. The time-dependent average number of photons in both field modes (total signal) obtained in dependence on phase ϕ (a) for qubit interacting with only input field mode ($\Gamma_2 = 0$); (b) for equal interaction of qubit with both fields $\Gamma_1 = \Gamma_2$. The input state corresponds to the state (15) with $\gamma = \beta = 1/\sqrt{2}$.

The described phase measurement does not require any information about the time-dependent photon statistics in the fields. It is based only on the joint measurement of the total signal (total intensity) in both field modes, which can be determined with high precision in an experiment. Thus, the proposed scheme of qubit-field interaction allows to perform highly sensitive measurements of the unknown relative phase of the input field state. In fact, this possibility is due to the anticorrelations of photons in the field modes arising during the interaction with the qubit.

5. Conclusion

In order to analyze the operation of a quantum element controlling non-classical fields, we have developed methods for the analytical consideration of the evolution of this complex system. The tools used in this article allow us to restore the amplitudes of all states of a multilevel composite system ("SA+F") along a chain of equations. The proposed splitting of a set of differential equations into subsets is particularly relevant when considering more complex all-quantum computing systems with large numbers of solid-state qubits (or qudits) and non-classical fields.

The developed tool made it possible to consider the control of non-classical fields for both weak and strong interaction of the resonators with an artificial atom for realistic conditions obtained from preliminary experiments.

In particular, we have demonstrated that a quantum controller can efficiently transmit the number of photons in the field from the input to the output when the frequency of the qubit is strongly detuned from the frequencies of the incident and outgoing waves. Of particular note is that superconducting technology allows not only the frequency of the qubit to be tuned, but also the frequencies of the waveguides.[73,74]

It is also possible to obtain the statistics of a nonclassical field by stopping the interaction between the qubit and the field at some point in time.

New states can also be created. Solid-state qubits can act as beam splitters for coherent fields by generating pure states of two less intense coherent fields. If the Fock state is at the input, entangled noon states can be generated. Finally, two fields at the input of the qubit allow the output signal to be stabilized for a noticeable period of time.

By considering a finite qubit anharmonicity and the actual multilevel transmon structure, many frequency field modes can be involved in the interaction. The control of the dominant coupling between different transmon levels is expected by changing the field frequencies and varying the degree of nonlinearity. In this case, the multilevel transmon can act as a multimode field converter.

In the future, within the framework of the proposed approach, a solid-state qubit can be considered as a quantum router that forms the populations of specific Fock (field) states acting as information transmission channels. Multiplexing a signal in the domain of Fock states (by analogy with frequency or time multiplexing) can be very important when working with data flows between quantum computing systems or matrices of quantum detectors.

Acknowledgements

The analytical and numerical study of the dynamics of states in a quantum controller was supported by the Foundation for Theoretical Physics and Mathematics, grant number 21-1-5-32-1. The concept of hybrid quantum computers using both solid-state and flying qubits (Section 1) was developed with support from RSF grant 20-12-00130. The study of the basic element for quantum networking (Section 2) is supported by Ministry of Science and Higher Education of the Russian Federation (agreement No. 075-15-2024-538). The work of D.S.Ya was supported by ANR JCJC (HECTOR 308 ANR-21-CE47-0002-01) and by Thales through a Co-fund PhD fellowship.

Conflict of Interest

The authors declare no conflict of interest.

Author Contributions

All of the authors discussed the results and their implications equally.

Data Availability Statement

The data that support the findings of this study are available from the corresponding author upon reasonable request.

Keywords

non-classical field, quantum communication, qubits, superconducting resonators

Received: March 30, 2024
Revised: June 9, 2024
Published online: July 3, 2024

[1] R. P. Feynman, in *Feynman and computation*, CRC Press, **2018**, pp. 133–153., *21*.
[2] L. K. Grover, in *Proceedings of the twenty-eighth annual ACM symposium on Theory of computing*, ACM, Inc., Philadelphia PA, USA **1996**, pp. 212–219.
[3] P. W. Shor, *SIAM Rev.* **1999**, *41*, 303.
[4] G. Q. AI, *Nature* **2023**, *614*, 676.
[5] Y. Nakamura, Y. A. Pashkin, J. Tsai, *Nature* **1999**, *398*, 786.
[6] J. Mooij, T. Orlando, L. Levitov, L. Tian, C. H. Van der Wal, S. Lloyd, *Science* **1999**, *285*, 1036.
[7] J. M. Martinis, S. Nam, J. Aumentado, C. Urbina, *Phys. Rev. Lett.* **2002**, *89*, 117901.
[8] D. Vion, A. Aassime, A. Cottet, P. Joyez, H. Pothier, C. Urbina, D. Esteve, M. H. Devoret, *Science* **2002**, *296*, 886.
[9] I. Chiorescu, Y. Nakamura, C. M. Harmans, J. Mooij, *Science* **2003**, *299*, 1869.
[10] J. Clarke, F. K. Wilhelm, *Nature* **2008**, *453*, 1031.
[11] J. M. Martinis, *Quantum Inf. Process.* **2009**, *8*, 81.
[12] V. E. Manucharyan, J. Koch, L. I. Glazman, M. H. Devoret, *Science* **2009**, *326*, 113.
[13] T. D. Ladd, F. Jelezko, R. Laflamme, Y. Nakamura, C. Monroe, J. L. O'Brien, *Nature* **2010**, *464*, 45.
[14] J.-Q. You, F. Nori, *Nature* **2011**, *474*, 589.
[15] P. Krantz, M. Kjaergaard, F. Yan, T. P. Orlando, S. Gustavsson, W. D. Oliver, *Appl. Phys. Rev.* **2019**, *6*, 021318.
[16] Z. Velluire-Pellat, E. Maréchal, N. Moulonguet, G. Saïz, G. Ménard, S. Kozlov, F. Couëdo, P. Amari, C. Medous, J. Paris, R. Hostein, J. Lesueur, C. Feuillet-Palma, N. Bergeal, *Sci. Rep.* **2023**, *13*, 14366.
[17] F. Arute, K. Arya, R. Babbush, D. Bacon, J. C. Bardin, R. Barends, R. Biswas, S. Boixo, F. G. Brandao, D. A. Buell, B. Burkett, Y. Chen, Z. Chen, B. Chiaro, R. Collins, W. Courtney, A. Dunsworth, E. Farhi, B. Foxen, A. Fowler, C. Gidney, M. Giustina, R. Graff, K. Guerin, S. Habegger, M. P. Harrigan, M. J. Hartmann, A. Ho, M. Hoffmann, T. Huang, et al., *Nature* **2019**, *574*, 505.
[18] M. Kjaergaard, M. E. Schwartz, J. Braumüller, P. Krantz, J. I.-J. Wang, S. Gustavsson, W. D. Oliver, *Annu. Rev. Condens. Matter Phys.* **2020**, *11*, 369.
[19] J. Zotova, S. Sanduleanu, G. Fedorov, R. Wang, J. S. Tsai, O. Astafiev, *Appl. Phys. Lett.* **2024**, *124*, 10.
[20] I. N. Moskalenko, I. A. Simakov, N. N. Abramov, A. A. Grigorev, D. O. Moskalev, A. A. Pishchimova, N. S. Smirnov, E. V. Zikiy, I. A. Rodionov, I. S. Besedin, *npj Quantum Inf.* **2022**, *8*, 130.
[21] A. Wallraff, D. I. Schuster, A. Blais, L. Frunzio, R.-S. Huang, J. Majer, S. Kumar, S. M. Girvin, R. J. Schoelkopf, *Nature* **2004**, *431*, 162.
[22] J. Gambetta, A. Blais, D. I. Schuster, A. Wallraff, L. Frunzio, J. Majer, M. H. Devoret, S. M. Girvin, R. J. Schoelkopf, *Phys. Rev. A* **2006**, *74*, 042318.
[23] A. Blais, A. L. Grimsmo, S. M. Girvin, A. Wallraff, *Rev. Mod. Phys.* **2021**, *93*, 025005.
[24] L. Lu, X. Zheng, Y. Lu, S. Zhu, X.-S. Ma, *Adv. Quantum Technol.* **2021**, *4*, 2100068.
[25] V. A. Vozhakov, M. V. Bastrakova, N. V. Klenov, I. I. Soloviev, W. V. Pogosov, D. V. Babukhin, A. A. Zhukov, A. M. Satanin, *Phys.-Uspekhi* **2022**, *65*, 457.
[26] A. Ranadive, M. Esposito, L. Planat, E. Bonet, C. Naud, O. Buisson, W. Guichard, N. Roch, *Nat. Commun.* **2022**, *13*, 1737.
[27] O. Milul, B. Guttel, U. Goldblatt, S. Hazanov, L. M. Joshi, D. Chausovsky, N. Kahn, E. Çiftyürek, F. Lafont, S. Rosenblum, *PRX Quantum* **2023**, *4*, 030336.
[28] A. L. Grimsmo, A. Blais, *npj Quantum Inf.* **2017**, *3*, 20.
[29] L. Fasolo, A. Greco, E. Enrico, F. Illuminati, R. L. Franco, D. Vitali, P. Livreri, *Measur.: Sens.* **2021**, *18*, 100349.
[30] Z. Peng, S. De Graaf, J. Tsai, O. Astafiev, *Nat. Commun.* **2016**, *7*, 12588.
[31] Y. Zhou, Z. Peng, Y. Horiuchi, O. Astafiev, J. Tsai, *Phys. Rev. Appl.* **2020**, *13*, 034007.
[32] A. A. Sokolova, G. P. Fedorov, E. V. Il'ichev, O. Astafiev, *Phys. Rev. A* **2021**, *103*, 013718.
[33] D. Ilin, A. V. Poshakinskiy, A. N. Poddubny, I. Iorsh, *Phys. Rev. Lett.* **2023**, *130*, 023601.
[34] D. Shapiro, A. Zhukov, W. Pogosov, Y. E. Lozovik, *Phys. Rev. A* **2015**, *91*, 063814.
[35] B. Kannan, M. J. Ruckriegel, D. L. Campbell, A. Frisk Kockum, J. Braumüller, D. K. Kim, M. Kjaergaard, P. Krantz, A. Melville, B. M. Niedzielski, A. Vepsäläinen, R. Winik, J. Yoder, F. Nori, T. P. Orlando, S. Gustavsson, W. D. Oliver, *Nature* **2020**, *583*, 775.
[36] G. Fedorov, S. Remizov, D. Shapiro, W. Pogosov, E. Egorova, I. Tsitsilin, M. Andronik, A. Dobronosova, I. Rodionov, O. Astafiev, A. V. Ustinov, *Phys. Rev. Lett.* **2021**, *126*, 180503.
[37] S.-H. Tan, B. I. Erkmen, V. Giovannetti, S. Guha, S. Lloyd, L. Maccone, S. Pirandola, J. H. Shapiro, *Phys. Rev. Lett.* **2008**, *101*, 253601.
[38] E. Lopaeva, I. R. Berchera, I. P. Degiovanni, S. Olivares, G. Brida, M. Genovese, *Phys. Rev. Lett.* **2013**, *110*, 153603.
[39] Z. Zhang, S. Mouradian, F. N. Wong, J. H. Shapiro, *Phys. Rev. Lett.* **2015**, *114*, 110506.
[40] P. Kurpiers, P. Magnard, T. Walter, B. Royer, M. Pechal, J. Heinsoo, Y. Salathé, A. Akin, S. Storz, J.-C. Besse, S. Gasparinetti, A. Blais, A. Wallraff, *Nature* **2018**, *558*, 264.
[41] A. S. Cacciapuoti, M. Caleffi, F. Tafuri, F. S. Cataliotti, S. Gherardini, G. Bianchi, *IEEE Network* **2019**, *34*, 137.
[42] P. Magnard, S. Storz, P. Kurpiers, J. Schär, F. Marxer, J. Lütolf, T. Walter, J.-C. Besse, M. Gabureac, K. Reuer, A. Akin, B. Royer, A. Blais, A. Wallraff, *Phys. Rev. Lett.* **2020**, *125*, 260502.
[43] M. Pompili, S. L. Hermans, S. Baier, H. K. Beukers, P. C. Humphreys, R. N. Schouten, R. F. Vermeulen, M. J. Tiggelman, L. dos Santos Martins, B. Dirkse, S. Wehner, R. Hanson, *Science* **2021**, *372*, 259.
[44] Y. Zhong, H.-S. Chang, A. Bienfait, É. Dumur, M.-H. Chou, C. R. Conner, J. Grebel, R. G. Povey, H. Yan, D. I. Schuster, A. N. Cleland, *Nature* **2021**, *590*, 571.
[45] A. Singh, K. Dev, H. Siljak, H. D. Joshi, M. Magarini, *IEEE Commun. Surv. Tutor.* **2021**, *23*, 2218.
[46] A. Somoroff, P. Truitt, A. Weis, J. Bernhardt, D. Yohannes, J. Walter, K. Kalashnikov, M. Renzullo, R. A. Mencia, M. G. Vavilov, V. E. Manucharyan, I. V. Vernik, O. Mukhanov, *Phys. Rev. Appl.* **2024**, *21*, 024015.
[47] M. Neeley, M. Ansmann, R. C. Bialczak, M. Hofheinz, E. Lucero, A. D. O'Connell, D. Sank, H. Wang, J. Wenner, A. N. Cleland, M. R. Geller, J. M. Martinis, *Science* **2009**, *325*, 722.
[48] E. Kiktenko, A. Fedorov, A. Strakhov, V. Man'Ko, *Phys. Lett. A* **2015**, *379*, 1409.
[49] S. Choi, J. Choi, R. Landig, G. Kucsko, H. Zhou, J. Isoya, F. Jelezko, S. Onoda, H. Sumiya, V. Khemani, C. von Keyserlingk, N. Y. Yao, E. Demler, M. D. Lukin, *Nature* **2017**, *543*, 221.
[50] V. Parigi, V. D'Ambrosio, C. Arnold, L. Marrucci, F. Sciarrino, J. Laurat, *Nat. Commun.* **2015**, *6*, 7706.
[51] F. Meng, L. Cao, J. Mangeney, H. G. Roskos, *Nanophotonics* **2024**, *13*, 2443.
[52] D.-S. Ding, W. Zhang, S. Shi, Z.-Y. Zhou, Y. Li, B.-S. Shi, G.-C. Guo, *Light: Sci. Appl.* **2016**, *5*, e16157.
[53] D. Cozzolino, B. Da Lio, D. Bacco, L. K. Oxenløwe, *Adv. Quantum Technol.* **2019**, *2*, 1900038.
[54] D. Subero, O. Maillet, D. S. Golubev, G. Thomas, J. T. Peltonen, B. Karimi, M. Marin-Suarez, A. L. Yeyati, R. Sanchez, S. Park, J. P. Pekola, *Nat. Commun.* **2023**, *14*, 7924.

[55] M. Erhard, M. Krenn, A. Zeilinger, *Nat. Rev. Phys.* **2020**, *2*, 365.
[56] H.-H. Lu, Z. Hu, M. S. Alshaykh, A. J. Moore, Y. Wang, P. Imany, A. M. Weiner, S. Kais, *Adv. Quantum Technol.* **2020**, *3*, 1900074.
[57] S. Danilin, A. V. Lebedev, A. Vepsäläinen, G. B. Lesovik, G. Blatter, G. Paraoanu, *npj Quantum Inf.* **2018**, *4*, 29.
[58] S. Danilin, N. Nugent, M. Weides, *New J. Phys.* **2024**.
[59] D. F. Walls, M. J. Collet, G. J. Milburn, *Phys. Rev. D* **1985**, *32*, 3208.
[60] A. Y. Dmitriev, R. Shaikhaidarov, T. Hönigl-Decrinis, S. De Graaf, V. Antonov, O. Astafiev, *Phys. Rev. A* **2019**, *100*, 013808.
[61] W. V. Pogosov, A. Y. Dmitriev, O. V. Astafiev, *Phys. Rev. A* **2021**, *104*, 023703.
[62] R. Barends, J. Kelly, A. Megrant, D. Sank, E. Jeffrey, Y. Chen, Y. Yin, B. Chiaro, J. Mutus, C. Neill, P. O'Malley, P. Roushan, J. Wenner, T. C. White, A. N. Cleland, John M. Martinis, *Phys. Rev. Lett.* **2013**, *111*, 080502.
[63] M. A. Aamir, C. C. Moreno, S. Sundelin, J. Biznárová, M. Scigliuzzo, K. E. Patel, A. Osman, D. Lozano, I. Strandberg, S. Gasparinetti, *Phys. Rev. Lett.* **2022**, *129*, 123604.
[64] J. Koch, M. Y. Terri, J. Gambetta, A. A. Houck, D. I. Schuster, J. Majer, A. Blais, M. H. Devoret, S. M. Girvin, R. J. Schoelkopf, *Phys. Rev. A* **2007**, *76*, 042319.
[65] M. D. Reed, B. R. Johnson, A. A. Houck, L. DiCarlo, J. M. Chow, D. I. Schuster, L. Frunzio, R. J. Schoelkopf, *Appl. Phys. Lett.* **2010**, *96*, 20.
[66] T. E. Roth, W. C. Chew, *IEEE J. Multiscale Multiphys. Comput. Tech.* **2022**, *7*, 92.
[67] D.-R. W. Yost, M. E. Schwartz, J. Mallek, D. Rosenberg, C. Stull, J. L. Yoder, G. Calusine, M. Cook, R. Das, A. L. Day, E. B. Golden, D. K. Kim, A. Melville, B. M. Niedzielski, W. Woods, A. J. Kerman, W. D. Oliver, *npj Quantum Inf.* **2020**, *6*, 59.
[68] T. M. Hazard, W. Woods, D. Rosenberg, R. Das, C. F. Hirjibehedin, D. K. Kim, J. Knecht, J. Mallek, A. Melville, B. M. Niedzielski, K. Serniak, K. M. Sliwa, D. R. W. Yost, J. L. Yoder, W. D. Oliver, M. E. Schwartz, *Appl. Phys. Lett.* **2023**, *123*, 154004.
[69] F. Lecocq, I. M. Pop, Z. Peng, I. Matei, T. Crozes, T. Fournier, C. Naud, W. Guichard, O. Buisson, *Nanotechnology* **2011**, *22*, 315302.
[70] D. O. Moskalev, E. V. Zikiy, A. A. Pishchimova, D. A. Ezenkova, N. S. Smirnov, A. I. Ivanov, N. D. Korshakov, I. A. Rodionov, *Sci. Rep.* **2023**, *13*, 4174.
[71] M. Mirhosseini, E. Kim, V. S. Ferreira, M. Kalaee, A. Sipahigil, A. J. Keller, O. Painter, *Nat. Commun.* **2018**, *9*, 3706.
[72] G. S. Mazhorin, I. N. Moskalenko, I. S. Besedin, D. S. Shapiro, S. V. Remizov, W. V. Pogosov, D. O. Moskalev, A. A. Pishchimova, A. A. Dobronosova, I. Rodionov, A. V. Ustinov, *Phys. Rev. A* **2022**, *105*, 033519.
[73] I. Siddiqi, *Nat. Rev. Mater.* **2021**, *6*, 875.
[74] Y. Sunada, K. Yuki, Z. Wang, T. Miyamura, J. Ilves, K. Matsuura, P. A. Spring, S. Tamate, S. Kono, Y. Nakamura, *PRX Quantum* **2024**, *5*, 010307.